(GRANT AGREEMENT: 661880)

DELIVERABLE D1.4

A Report of Uranium(VI) Speciation Associated with Cellulose Degradation Products

H. Brinkmann[1], H. Moll[1], M. Patzschke[1], P. Kaden[1], T. Arnold[1]

1. Helmholtz-Zentrum Dresden-Rossendorf (HZDR), Germany

Date of issue of this report: **30/06/2018**

Start date of project: 01/06/15 Duration: 37 Months

This project has received funding from the Euratom research and training programme 2014-2018 under Grant Agreement no. 661880		
Dissemination Level		
PU	Public	**x**
RE	Restricted to a group specified by the partners of the MIND project project	
CO	Confidential, only for partners of the MIND project	

Publishable Summary

Work Package 1 of the MIND project addresses remaining key issues for the geological disposal of ILW concerning the long-term behaviour, fate and consequences of organic materials in the waste along with H_2 generated by corrosion and radiolysis. Degradation products of organic components in nuclear waste can enter the environmental water pathways. They can act as complexing agents for released radionuclides. Thereby they can increase the concentration of radionuclides in environmental waters. Hence, a mobilization of toxic radionuclides can take place. This report deals with a detailed characterization of the uranium(VI) speciation in the presence of acetate and isosaccharinic acid (HISA) mainly by applying spectroscopic techniques. The motivation for this study was to provide spectroscopic parameters such as absorption-, luminescence- and infrared spectra as well as structural data, for each uranyl complex, which can then serve as reference data. It was further important to work with low, environmentally relevant uranium concentrations. Especially in the uranium(VI)-acetate system, it was difficult and partially not reasonable to interpret the spectroscopic data with the formation of three uranyl-acetate complexes. For this reason, especially the studies focusing on the determination of the speciation were critically reviewed. The combination of experimental results of the present and crucial revelations in previous studies results in a different point of view on the aqueous uranyl-acetate system. Moreover, the fate of uranium in a long-term tissue degradation experiment under hyperalkaline conditions was investigated.

The report will provide a basis for the new interpretation of soluble U(VI) species in the presence of acetate and isosaccharinate (ISA) as main products of cellulose degradation. This impacts also the modelling of U(VI) dissemination from nuclear waste repositories.

Contents

List of Figures

The MIND-project has received funding from the European Union's EUROATOM research and training program (Horizon2020) under grant agreement 661880.

The MIND-project has received funding from the European Union's EUROATOM research and training program (Horizon2020) under grant agreement 661880.

List of Tables

The MIND-project has received funding from the European Union's EUROATOM research and training program (Horizon2020) under grant agreement 661880.

1 Introduction

1.1 Characterization of organic degradation products and interaction with radionuclides

A comprehensive review concerning the organic compounds in nuclear waste and their degradation behaviour was prepared by several partners of the MIND-project.(*1*) Small water soluble organic compounds, like organic degradation products, can act as complexing agents for radionuclides and can potentially increase their solubility and decrease their sorption on engineered barriers or the host rock. In the context of nuclear waste disposal, it is essential to know the relative stabilities of the compounds and complexes that may form under relevant conditions, in order to model the behaviour of actinides and fission products under environmental conditions.(*2*) To assess the safety of a nuclear waste repository, it is therefore necessary to gather a fundamental knowledge about the speciation of radionuclides under environmentally relevant conditions, and therefore also in the presence of organic degradation products.

1.2 Degradation of cellulose under alkaline conditions

Cellulose is present in LILW in considerable amounts and will be relatively fast degraded under alkaline conditions. The degradation mechanism, starting from the reducing end of the glucose-polymer, is shown in Figure 1, according to (*3*). Step (i) and (vi) are triggered by hydroxy-ions. This mechanism shows the formation of the main degradation-product isosaccharinic acid (HISA).

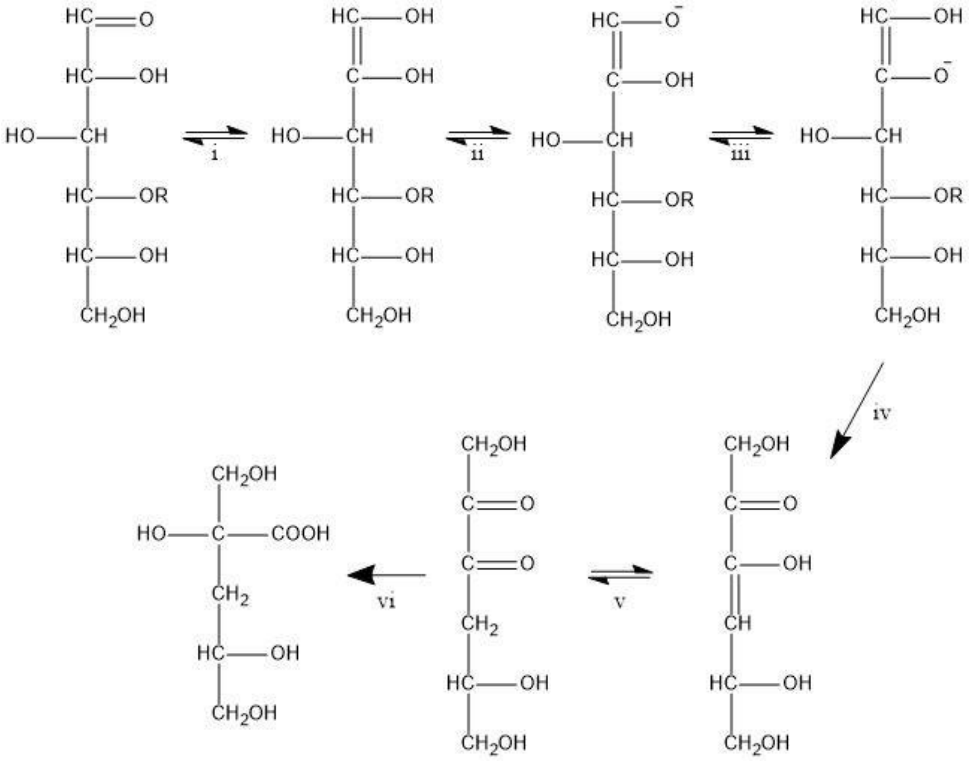

Figure 1: Cellulose degradation mechanism under alkaline conditions: (i) keto-enol tautomerism, (ii) enediol deprotonation, (iii) anion isomerisation, (iv) β-hydroxycarbonyl elimination, (v) keto-enol tautomerism, (vi) benzilic acid rearrangement.(*3*)

The MIND-project has received funding from the European Union's EUROATOM research and training program (Horizon2020) under grant agreement 661880.

Glaus *et al*. showed that up to 80% of the dissolved organic products, resulting from cellulose degradation, can be explained with the formation of HISA.(*4*) Additionally, several small carboxylic acids, including acetic acid, were formed.

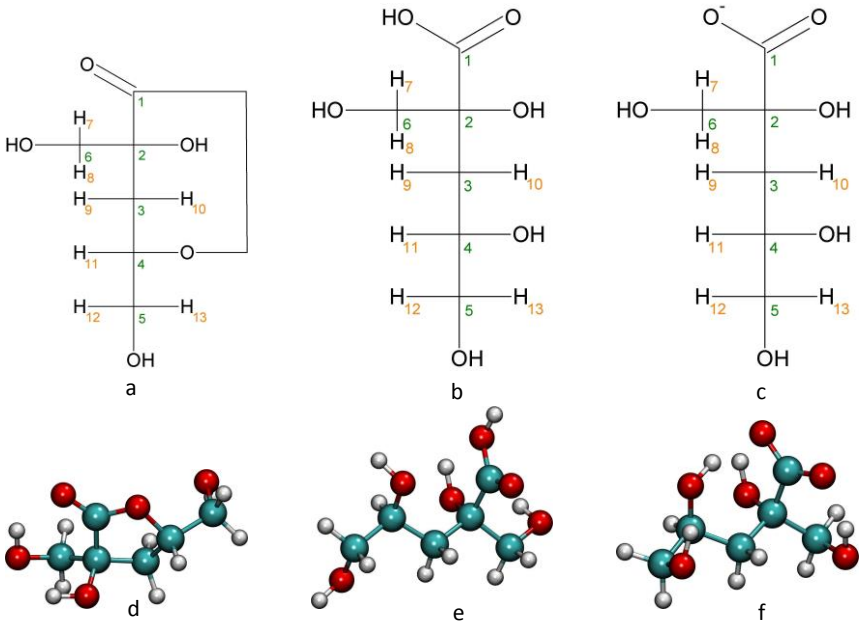

Figure 2: HISA-Conformations: Fischer projection of ISL (a), HISA (b), ISA (c) and their related optimized structures ((d), (e) (f)).

HISA is a polyhdroxy-carboxylic acid, which has a tertiary, secondary and two primary alcohols. The carboxylic group has a pK_A of 3.27.(*5*) Under very acidic conditions a ring-closing reaction occurs between C_1 and the secondary alcohol at C_4. This lactone form prevails under very acidic conditions.(*6*, *7*) HISA causes great concerns since it was shown that it forms complexes with several radionuclides and enhances their solubility and decreases their sorption. The knowledge about HISA-interaction with radionuclides in their stable oxidation states is limited.(*8*, *9*, *18*, *10*–*17*) Therefore, it is necessary to generate thermodynamic data as well as reference data related to the structural properties of the ligand to understand its behaviour, while acting as complexing agent. Especially in the case of uranium(VI), the number of studies is low. Rao *et al*. determined the formation of 1:1, 1:2 and 1:3 complexes under acidic conditions by potentiometry. In contrast to that postulated Warwick *et al*. the formation of a 1:1 complex under neutral conditions based on conductometric measurements. These contradictory statements have to be validated.

The MIND-project has received funding from the European Union's EUROATOM research and training program (Horizon2020) under grant agreement 661880.

2 Methods

2.1 Preparation of ISA

The synthesis of $Ca(ISA)_2$ was generally performed as described in (*19*, *20*) and (*21*). 500 ml di water were flushed with argon for 3 h in a 1 l round bottom flask. 50 g α-lactose monohydrate and 13.6 g $Ca(OH)_2$ were added under slight argon flush. The mixture was stirred moderately and flushed with argon. After 1 h the flask was closed and carefully sealed with parafilm. The suspension was stirred for 3 d at RT, whereby the color changed from bright white over yellow and orange to brown (Figure A 1).

After 3 d the brown solution was boiled under reflux for 6 h whereby the color changed to dark brown and black. The hot solution was filtered, and the volume was reduced to around 100 ml by boiling. Afterwards the filtered solution was stored at 4°C until a bright precipitate was formed. The solution was filtered, and the crude precipitate was washed with water and ethanol and subsequently dried at 50°C. 1.2 g of the crude precipitate was dissolved in 100 ml di water by boiling and the volume was reduced to 10 ml. The white precipitate was filtered and washed with water and ethanol (Figure A 2). This step was repeated, and the white powder was dried at 50°C. The yield was around 8 g per 50 g α-lactose monohydrate and the dry powder was stored in the dark at RT.

Since $Ca(ISA)_2$ has a low solubility in water the calcium was replaced by sodium using a cation exchange resin (Chelex BioRad 100) as described in (*22*). 4 g of $Ca(ISA)_2$ together with 100 g of Chelex-100 resin in the sodium form were stirred in 100 ml di water for 3 h. The suspension was centrifuged, and the supernatant was filtered to fully remove the resin. The volume of the filtrate was reduced to around 45ml by boiling, resulting in a brownish solution. Aliquots were taken for TOC analysis to determine the ISA concentration and for ICP-MS analysis to determine the content of sodium and calcium in solution. To verify the purity of NaISA stock solution ^{1}H- and ^{13}C-NMR spectra were measured and compared to the literature. Furthermore, ISA was characterized with ATR-FTIR-spectroscopy.

2.2 UV-vis-spectroscopy

UO_2^{2+}-ISA investigations were performed in standard 1 cm cuvettes since the concentrations above 10 mM were relatively high. The measurements were performed with a TIDAS 100 spectrometer. Deionized water was measured as background.

The concentrations in the UO_2^{2+}-Acetate experiments were much lower (50 µM). To overcome the small extinction coefficients in combination with low concentrations of uranyl species a World Precision Instruments Liquid Waveguide Capillary Cell (LWCC) with a path length of 250 cm was used. The LWCC was connected with optical fibers to a TIDAS 100 spectrometer. The absorption spectra were recorded between 280 and 600 nm with a resolution of 0.1 nm. Each time before a sample was measured a background measurement (deionized water) was performed to minimize the effect of the baseline drifts on the recorded spectra. The UV-vis spectra of the UO_2^{2+}-Acetate system were evaluated with HypSpec to obtain single component spectra as well as complex formation constants.(*23*)

2.3 Luminescence spectroscopy

The samples were excited with a pulsed Nd:YAG laser at 266 nm (Inlite laser system, Continuum, 20 Hz, 1090 V) and the static luminescence spectra were recorded with a CCD-camera (iHR550, Horiba Jobin Yvon). For time-resolved luminescence spectra, a certain number of spectra was recorded with increasing delay-time after the laser pulse. A sample holder, which allows the adjustment of the temperature, was used to measure the luminescence at 25°C. To minimize the quenching effects the samples were also measured at -120°C, which was realized with a setup described by Günther *et al.*.(*24*)

The MIND-project has received funding from the European Union's EUROATOM research and training program (Horizon2020) under grant agreement 661880.

2.4 ATR-FTIR-spectroscopy

ATR-FTIR-spectra were recorded as described in (*25*). A Bruker Vertex 80/v vacuum spectrometer equipped with a mercury cadmium telluride (MCT) detector was used. The applied ATR accessory was a horizontal diamond crystal with 9 internal reflections (DURA SamplIR II, Smiths Inc.). The ATR cell was purged with a current of dry air (dew point < 213 K). For adequate subtraction of the background spectrum, an ATR flow cell was used which allows an exchange of the sample solution without any external thermal perturbations of the equilibrated system.

2.5 NMR-spectroscopy

NMR-spectra were recorded on a Varian Inova 400 spectrometer frequencies for ^{1}H of 399.89 MHz and for ^{13}C of 100.56 MHz. All samples were measured at 298 K with a Varian PFG ID sample holder with z-gradient. Standard pulse-sequences of Agilent were applied to record the 1D and 2D spectra.

2.6 DFT-calculations

Structures were optimized based on the density functional theory (DFT), considering solvent effects with the conductor like screening model (COSMO). Scalar relativistic effects at the Uranium were considered with an effective core potential. The functional was BP86 and the basis set was def2-TZVPP.

The MIND-project has received funding from the European Union's EUROATOM research and training program (Horizon2020) under grant agreement 661880.

3 Interaction of UO_2^{2+} with acetate[1]

Pioneering work with respect to the interaction of the uranyl ion with acetate was done by Ahrland in 1951.(*26*) Based on potentiometric measurements he proposed the formation of three uranyl-acetate complexes with the metal to ligand ratio of 1:1, 1:2, and 1:3 under acidic conditions. In the following more than sixty years the number of related studies increased, and the uranyl-acetate system seemed to become a well understood system in terms of speciation, thermodynamics, as well as structural properties of the formed complexes, at least under acidic conditions.

The importance of direct and sensitive UV-vis and laser induced luminescence spectroscopic measurements in the analytical chemistry is unambiguous. Changes in the luminescence and absorption spectra of the uranyl ion were often used to determine the speciation in the system of interest. The resulting single component spectra, band positions and luminescence lifetimes were then used as reference data to interpret similar as well as more complex systems. Sladkov investigated the complexation of the uranyl ion with acetate and the quenching effects by time-resolved laser-induced luminescence spectroscopy.(*27*, *28*) Since he focused on the quenching effects and the formation of the 1:1-complex, the luminescence properties of the remaining uranyl-acetate complexes are still missing. Meinrath et al. determined the single component spectrum of the 1:1-complex, but again the spectra of the remaining complexes were not determined.(*29*) Other studies, which applied UV-vis spectroscopy, provided no specific characteristics for the different uranyl-acetate complexes (band positions and extinction coefficients).(*30*, *31*) The motivation for this study was to provide spectroscopic parameters, luminescence and absorption spectra, for each uranyl-acetate complex, which can then serve as reference data. It was further important to work with low, environmentally more relevant uranium concentrations.

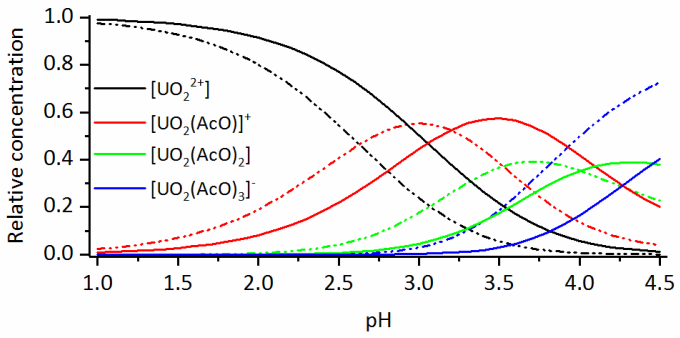

Figure 3: Calculated speciation diagrams under experimental conditions with 50 µM UO_2^{2+} and 0.1 M acetate (solid lines) or 0.3 M acetate (dashed lines).

Figure 3 shows the calculated speciation under experimental conditions. The calculation was performed using the geochemical speciation code PHREEQC (Version 3.4.12927) with the thermodynamic data of the OECA/NEA Thermochemical Database supplemented by thermodynamic data for the uranium(VI)-acetate complexation from Brown and Wanner. (*2*, *32*–*34*) All figures from experimental results shown in that section are from the test series with 0.1 M acetate.

[1] Some phrases and figures were directly adopted without changes from the manuscript: *Revision of the uranyl-acetate system: A new perspective based on spectroscopic measurements and a critical literature review*.

The MIND-project has received funding from the European Union's EUROATOM research and training program (Horizon2020) under grant agreement 661880.

3.1 TRLFS investigations

The course of the luminescence spectra at 25°C can be divided into two distinct phases (Figure 4a and c). As expected from the speciation calculation (Figure 3) the first spectrum can be unambiguously assigned to the pentaaquo-complex of the uranyl ion (Species 1). The related band positions are in very good agreement with literature values (Table 1).(*35*, *36*) Starting from that spectrum, the intensity decreases with increasing pH, which was caused by several factors. It was previously shown by Sladkov that the $[UO_2AcO]^-$-complex (Species 2, 1:1-complex) is not luminescent at ambient temperatures.(*27*) Furthermore, if the amount of Species 2 increases, the amount of Species 1 must decrease. The third factor is the increased dynamic quenching due to higher concentrations of acetate in solution. Figure 4b shows that the normalized spectra of the first phase are nearly congruent, except the slightly arise of shoulders, which are caused by the initial transition to phase 2. This underpins the assumption that the occurring changes were caused by the formation of only on Species. A similar pattern is present at -120°C (Figure 5). The congruence of the spectra with pH from 1.1 to 2.2 strengthens again the conclusion that only one species was formed during that phase.

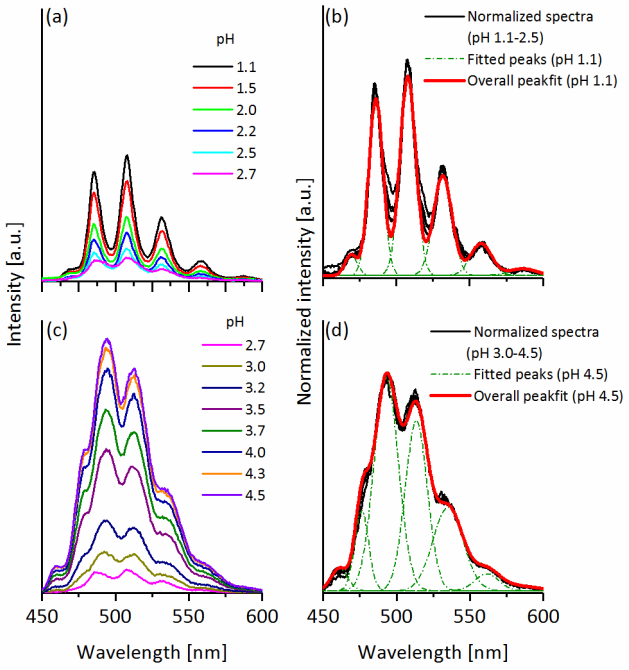

Figure 4: Luminescence spectra at 25°C. ***(a)*** *Phase 1: pH 1.1 to 2.2,* ***(b)*** *Normalized spectra of phase 1 (except pH 2.2) with the peak fit for the sample with pH 1.1,* ***(c)*** *Phase 2: pH 2.2 to 4.5,* ***(d)*** *Normalized spectra of phase 2 (except pH 2.2) with the peak fit for the sample with pH 4.5.*

In phase 2 a significant band shift as well as an increase in luminescence intensity occurs with increasing pH at both temperatures (Figure 4c and Figure 5a). The congruence of the normalized spectra of phase 2 again reveals that the changes are caused by the formation of a single species (Figure 4d and Figure 5c). Consequently, the determined band positions of Species 3 can be assigned to the second uranyl-acetate complex $[UO_2(AcO)_2]$ (1:2-complex). Even though the samples of both test series were prepared in way that all three uranyl-acetate complexes should be present, the luminescence spectra give no evidence for the formation of the third uranyl-acetate complex $[UO_2(AcO)_3]^+$ (Species 4, 1:3-complex).

The MIND-project has received funding from the European Union's EUROATOM research and training program (Horizon2020) under grant agreement 661880.

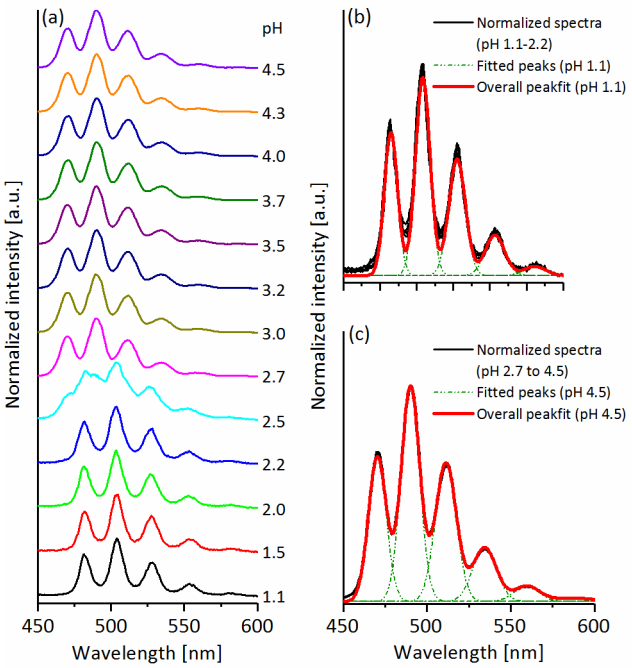

Figure 5: Luminescence spectra at -120°C. ***(a)*** *Normalized spectra,* ***(b)*** *Normalized spectra of phase 1 (except pH 2.2) with the peak fit for the sample with pH 1.1,* ***(c)*** *Normalized spectra of phase 2 (except pH 2.2) with the peak fit for the sample with pH 4.5.*

Table 1: Averaged luminescence maxima of test series 1 and 2 at 25°C and -120°C.

	Luminescence maxima in nm		
	This study (25°C)	**Reference (28°C)**	**This study (-120°C)**
Species 1 UO_2^{2+}	469.5, 486.4, 508.2, 531.9, 557.9, 586.0	470.2, 487.8, 509.3, 532.7, 558.1, 585.5 (*36*)	482.1, 503.8, 527.2, 553.0, 580.2
Species 2 $[UO_2AcO]^+$	-	-	-
Species 3 $[UO_2(AcO)_2]$	461.2, 476.4, 493.2, 513.7, 535.4, 561.5	-	470.8, 490.6, 511.8, 535.0, 560.1

3.1 UV-vis-spectroscopic investigations

In accordance with luminescence spectra, the course of the absorption spectra can be separated in two distinct phases (Figure 6). In phase 1 the absorption increases and the position of the initial maximum at 414.7 nm shifts to higher wavelengths with increasing pH (Figure 6a). These changes are accompanied with a loss of the characteristic vibrational structure of the absorption spectrum. The absorption slightly decreases with increasing pH in phase 2 (Figure 6b). In addition, a vibrational structure returns with the formation of distinct maxima. This general description would underpin the conclusion from luminescence measurements that only two instead of three uranyl-acetate complexes were formed.

To interpret the absorption data as unbiased as possible, the formation of on the one hand two uranyl-acetate complexes and on the other hand three uranyl-complexes was considered. For that purpose, the spectra of test series 1 and 2 were evaluated with HypSpec assuming three species (the uncomplexed uranyl ion, the 1:1-, and the 1:2-complex) for the first case and assuming the formation

The MIND-project has received funding from the European Union's EUROATOM research and training program (Horizon2020) under grant agreement 661880.

of a fourth species (the 1:3-complex) in the second case. The calculated single component spectra and stability constants of both test series were then averaged for each case (case 1: Figure 6c-e, Table 2; case 2: Figure 7, Table 3).

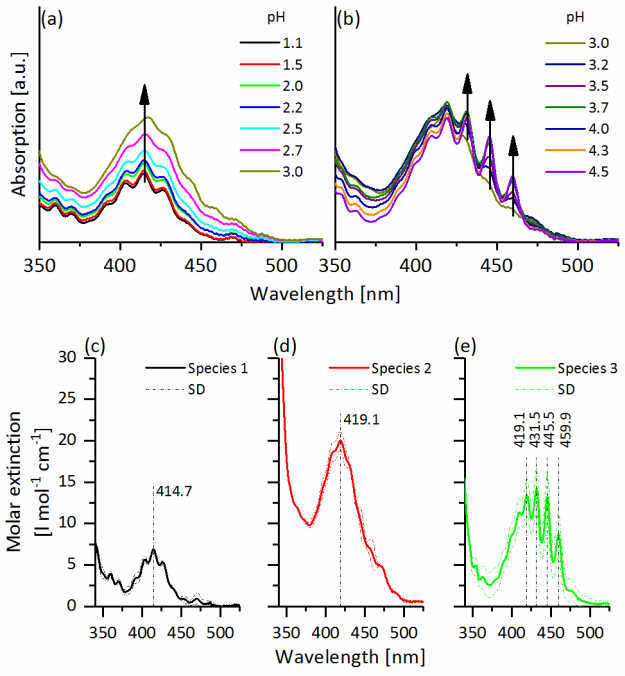

*Figure 6: Absorption spectra **(a and b)** and averaged single component spectra of UO_2^{2+} **(c)**, $[UO_2AcO)]^+$ **(d)** and $[UO_2(AcO)_2]$ **(e)**, considering three species.*

Table 2: Absorption maxima of averaged single component spectra and stability constants of test series 1 and 2, considering the formation of two complexes.

	Absorption maxima in nm (extinction coefficients in $mol \cdot l^{-1} \cdot cm^{-1}$)		*Averaged log β*
	This study	Reference	
Species 1 UO_2^{2+}	403.6, 414.7 (6.9 ± 0.0), 426.6	402.8, 414.6 (7.13 ± 0.1), 427.1(*36*)	
Species 2 $[UO_2AcO]^+$	419.1 (20.0 ± 1.0)	418.0 (17.8 ± 1.0)(*37*)	2.82 ± 0.18
Species 3 $[UO_2(AcO)_2]$	419.1, 431.5 (14.1 ± 2.5), 445.4, 459.9	-	4.86 ± 0.37

For the first case no constraints were necessary to fit the absorption spectra. Figure 6c-e show the resulting averaged single component spectra of the free uranyl ion (Species 1), the 1:1-complex (Species 2), and the 1:2-complex (Species 3) and its standard deviation (SD). The extinction coefficient as well as the absorption maximum of the uranyl ion are in a very good agreement with literature values (Table 2).(*36*) In addition does the single component spectrum of the 1:1-complex (Species 2) agree with the reported spectrum from Meinrath *et al.* in terms of the position of the absorption maximum and the related extinction coefficient.(*29*) The standard deviation in all three spectra is satisfactory.

The MIND-project has received funding from the European Union's EUROATOM research and training program (Horizon2020) under grant agreement 661880.

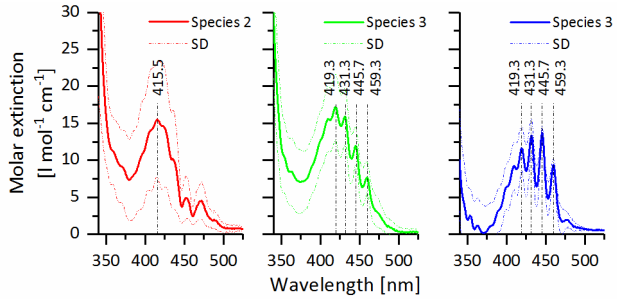

Figure 7: Averaged (series 1 and 2 evaluated with HypSpec) single component absorption spectra of species 2, 3 and 4, considering four species.

Table 3: Absorption maxima of averaged (test series 1 and 2 evaluated with HypSpec) single component spectra and stability constants, considering the formation of three complexes.

	Absorption maxima in nm (extinction coefficients in $mol \cdot l^{-1} \cdot cm^{-1}$)	Averaged log β
Species 2 $[UO_2AcO]^+$	415.5 (15.5 ± 7.6)	3.08 ± 0.70
Species 3 $[UO_2(AcO)_2]$	419.3 (17.2 ± 4.4)	5.90 ± 0.49
Species 4 $[UO_2(AcO)_3]^-$	445.7 (13.6 ± 0.9)	7.22 ± 0.74

To evaluate the test series assuming the formation of three uranyl-acetate species (case 2) it was necessary to fix the spectrum of the uranyl ion in test series 1. For that purpose, the spectrum of the sample with the lowest pH was chosen according to the calculated speciation. The enormous standard deviations of the calculated single component spectra for all three complexes (Figure 7) give rise to the assumption that something might be wrong. The single component spectrum of the 1:1-complex (Species 2) reveals significant deviations in terms of the absorption maximum and the related extinction coefficient compared to the reported spectrum from Meinrath *et al.*.(*37*) The spectra of Species 3 and 4 share the same absorption maxima and furthermore does the spectrum of Species 3 look like a transition from Species 2 to 4. All these crucial indications lead to the conclusion that the UV-vis data were over-interpreted considering a third uranyl-acetate complex.

3.2 Summary and Outlook

The fact that the luminescence as well as the absorption data can consistently be interpreted with the uranyl ion and the formation of two complexes is contradictory to the predicted speciation and the general opinion in the literature. It is for this reason necessary to critically review former studies, focusing on the determination of the number of formed uranyl-acetate complexes or rather the number of complexly bound acetate molecules per uranyl ion. Furthermore, additional methods, focusing on that issue could help to clarify this problem. Capillary electrophoresis was applied by Sladkov, but however he focused only on the 1:1 and 1:2 complex. This method seems to be very suitable, since these complexes have a different charge and should show a different electrophoretic mobility.

The MIND-project has received funding from the European Union's EUROATOM research and training program (Horizon2020) under grant agreement 661880.

4 Spectroscopic characterization of ISA

In order to use NMR- and ATR-FTIR-spectroscopy as methods for the detailed characterization of complexes, formed in the UO_2^{2+}-ISA system, it is necessary to provide reference data of the pure ligand. Therefore NaISA-solutions were characterized with these two methods in the absence of UO_2^{2+}. To understand the argumentation in the following sections, detectable carbon atoms and protons were labeled as depicted in Figure 8 (according to (*4*)).

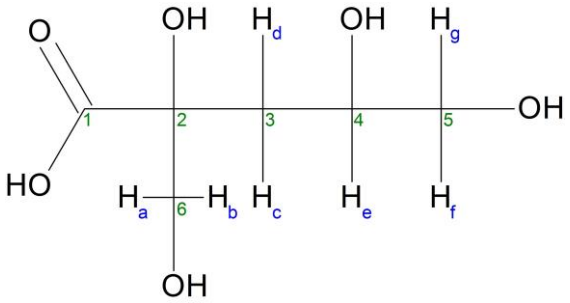

Figure 8: Structural formula of HISA with labeled carbon atoms and protons.

4.1 NMR-spectroscopy

To confirm the purity of synthesized ISA and to provide reference data for continuing experiments, 1D- (^{13}C and ^{1}H) and 2D-NMR measurements (HSQC and COSY) were performed. Therefore, a 50 mM NaISA-solution was prepared in D_2O (90%) and the pH was adjusted to 10.6. The resulting spectra are depicted in Figure A 3, Figure A 4, Figure A 5 and Figure A 6. Table 4 and Table 5 provide a summary of the chemical shifts and coupling constants in comparison with already published values. The experimentally determined ^{1}H-NMR signals and coupling constants are in very good agreement with values reported in (*4*). However, the values of the present study show an almost constant shift of 0.90(6) ppm compared to Glaus *et al.* This shift might be caused by the fact that the reference used here was TMSP, whereas Glaus et al. used the solvent signal of either water or acetone as internal standard. The mean of the deviations of the coupling constants is 0.06(5) Hz.

Table 4: Experimental and literature ^{1}H-NMR chemical shifts of ISA.

Proton	Multiplicity	Experimental chemical shift in ppm (coupling constant in Hz)	Chemical shift in ppm (coupling constant in Hz) from (*4*)
c/d	dd/dd	1.85 (14.5, 7.8)/1.69 (14.6, 4.8)	1.76 (14.5, 7.8)/1.61 (14.5, 4.7)
f/g	dd/dd	3.46 (11.8, 7.1)/3.62 (11.8, 3.7)	3.37 (11.7, 7.0)/3.53 (11.7, 3.7)
a/b	d/d	3.53 (11.4)/3.72 (11.5)	3.43 (11.4)/3.63 (11.4)
e	m	3.88 (7.9, 4.2)	3.79

The ^{13}C-NMR spectrum shows six signals (Figure A 4), representing the six carbon atoms of the ISA-molecule. Comparison of the measured signals with literature values reveals an almost constant difference of 2.9(1) ppm. This might be again caused by the different compounds, which were used as standard (TMSP or acetone). However, since no other signals were detected in the 1D-NMR-

The MIND-project has received funding from the European Union's EUROATOM research and training program (Horizon2020) under grant agreement 661880.

spectra and since the 2D-NMR-spectra reveal only couplings, being consistent with the structural properties of ISA, the purity of the synthesized NaISA stock solution can be estimated as >95%.

Table 5: Experimental and literature ^{13}C NMR chemical shifts of ISA.

Carbon	Experimental chemical shift in ppm	Chemical shift in ppm from (*38*)
3	40.5	37.6
5	68.9	66.0
6	70.7	67.9
4	71.2	68.4
2	80.4	77.8
1	182.8	180.0

4.2 ATR-FTIR-spectroscopy

Whereas several studies reported NMR-data for ISA and its conformations, no references are available for IR-data. To obtain these essential information, ATR-FTIR-spectra of 90 mM NaISA-solutions at different pH values were measured (see Figure A 7) and ITFA(*39*) was applied to calculate the single component vibrational spectra of ISL, HISA and ISA (see Figure 9). Based on literature values for (hydroxy-)carboxylic acids and lactones, the most important and prominent bands were assigned to the vibrations of related functional groups (see Table 6).(*40–44*) Figure A 8 shows the distribution of the components in the test solutions.

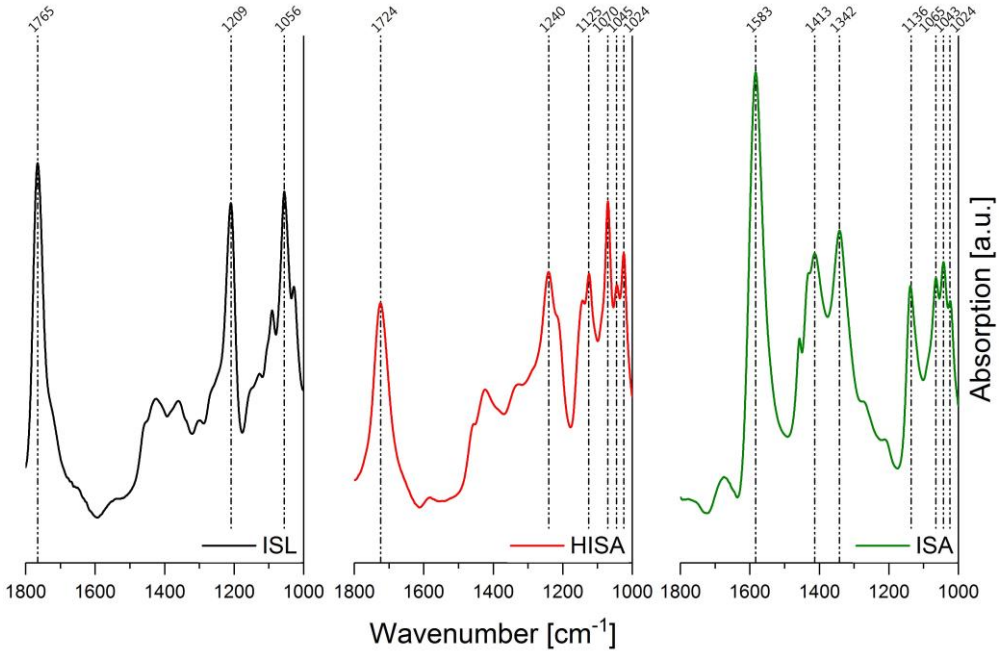

Figure 9: Single component ATR-FTIR-spectra of ISL, HISA and ISA.

The MIND-project has received funding from the European Union's EUROATOM research and training program (Horizon2020) under grant agreement 661880.

Table 6: Vibrational modes of ISL, HISA and ISA in solution in the range of 1800 cm^{-1} to 1000 cm^{-1}.

Compound	Frequencies in cm^{-1}	Assignments [a]
ISL	1765	$st_{C—O}$
	1209	asy $st_{C–O–C}$
	1056	sy $st_{C–O–C}$
HISA	1724	$st_{C—O}$
	1240	$st_{C–O^{ac}}$
	1125	$st_{C–O_{3°alc}}$
	1070	$st_{C–O_{2°alc}}$
	1045/1024	$st_{C–O_{1°alc}}$
ISA	1583	asy st_{COO^-}
	1413	sy st_{COO^-}
	1342	r_{CH_2} + sc_{CH_2} + $b_{O–H_{alc}}$
	1136	$st_{C–O_{3°alc}}$
	1065	$st_{C–O_{2°alc}}$
	1043/1024	$st_{C–O_{1°alc}}$

[a] Abbreviations: asy: antisymmetric; sy: symmetric; st, stretch; r: rock; sc: scissors; b: bend ac: acid; 1°, 2° and 3° alc: primary, secondary and tertiary alcohol

The MIND-project has received funding from the European Union's EUROATOM research and training program (Horizon2020) under grant agreement 661880.

5 Interaction of UO_2^{2+} with α-Isosaccharinic acid

5.1 Determination of the number of formed complexes

In order to determine the number of formed complexes between UO_2^{2+} and ISA, changes of the absorption spectra with changing pH, at different metal to ligand ratios were measured. Even the evaluation of the raw spectra in Figure 10 without the application of any mathematical procedure provides important information. Four distinct absorption maxima at 414 nm, 422 nm, 427 nm and 438 nm can be determined. Whereas the first species, showing a maximum at 414 nm, can unambiguously be assigned to the $[UO_2(H_2O)_5]^{2+}$-complex (*36*), the remaining maxima indicate the formation of three different UO_2^{2+}-ISA-complexes. Another striking observation is the strongly increasing absorption within the test series with increasing pH. The formation of the $[(UO_2)_2(OH)_2]^{2+}$- and $[(UO_2)_3(OH)_5]^{+}$-complexes show also a very strong absorption with maxima at 421.8 nm and 424.1 nm (*45*, *46*). However, the different absorption maxima argue against the formation of pure UO_2^{2+}-hydroxo species in the presence of ISA. Nevertheless, the strong absorption could be a crucial indication for the formation of polynuclear complexes between UO_2^{2+} and ISA.

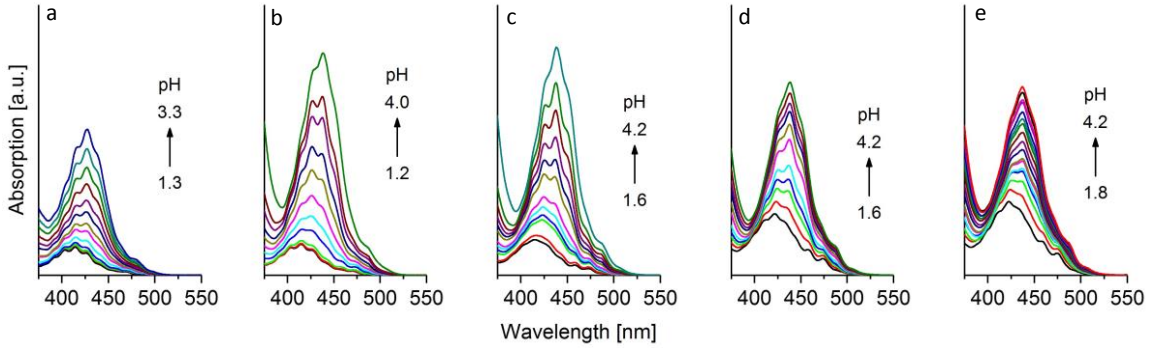

Figure 10: UV-vis-spectra of pH-series at different UO_2^{2+} (15 mM) to ISA ratios: 2:1 (a), 1:1 (b), 1:2 (c), 1:6 (d) and 1:16 (e).

ITFA was used to properly evaluate these data sets (*39*). The measured spectra in Figure 10 could be fairly good reproduced with four components and the distribution within the test series is depicted in Figure 11. Several observations have to be emphasized. Species 4 became more dominant, the higher the excess of ISA was. In contrast to that was the amount of Species 3 lowered, at higher ISA concentrations. Furthermore, was the formation of that component suppressed by the formation of Species 2, which was present at lower pH values and became more dominant the higher the excess of ISA was.

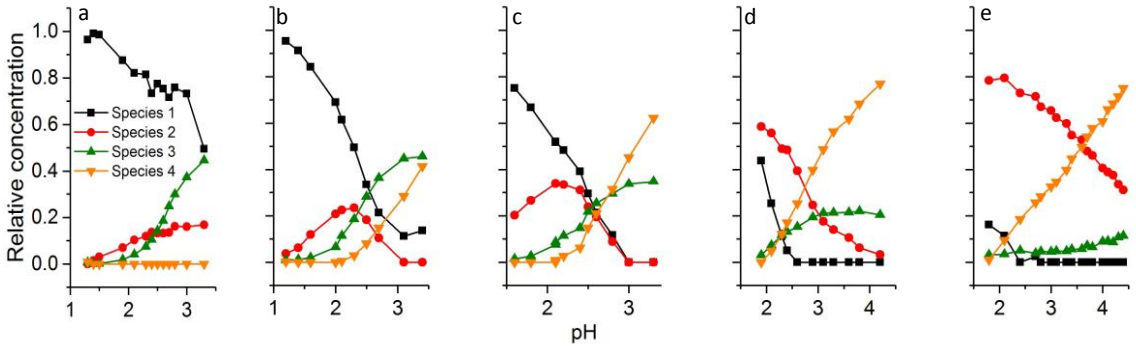

Figure 11: Relative concentrations derived from ITFA of UV-vis test series: 2:1 (a), 1:1 (b), 1:2 (c), 1:6 (d) and 1:16 (e).

The MIND-project has received funding from the European Union's EUROATOM research and training program (Horizon2020) under grant agreement 661880.

In addition to the concentration profiles of the four components, the corresponding single component absorption spectra were calculated with ITFA, which are shown in Figure 12. The previously mentioned high absorption could be verified for Species 3 and 4, but not for Species 2. These single component spectra are very valuable for continuing experiments, since UV-vis-spectroscopy could now be used as reference method.

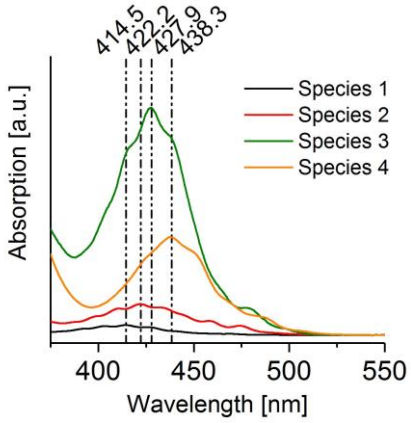

Figure 12: ITFA derived single component spectra of species in the UO_2^{2+}-ISA system.

This principle is shown in Figure 13. Four samples were prepared, containing 15 mM UO_2^{2+}, and the UV-vis-spectra confirmed, that always one of the four species is dominant in a certain sample. The corresponding luminescence spectra confirmed the presence of four species, having their luminescence maxima at 507.9 nm (Species 1), 513.2 nm (Species 2), 497.2 nm (Species 3) and 502.5 nm (Species 4).

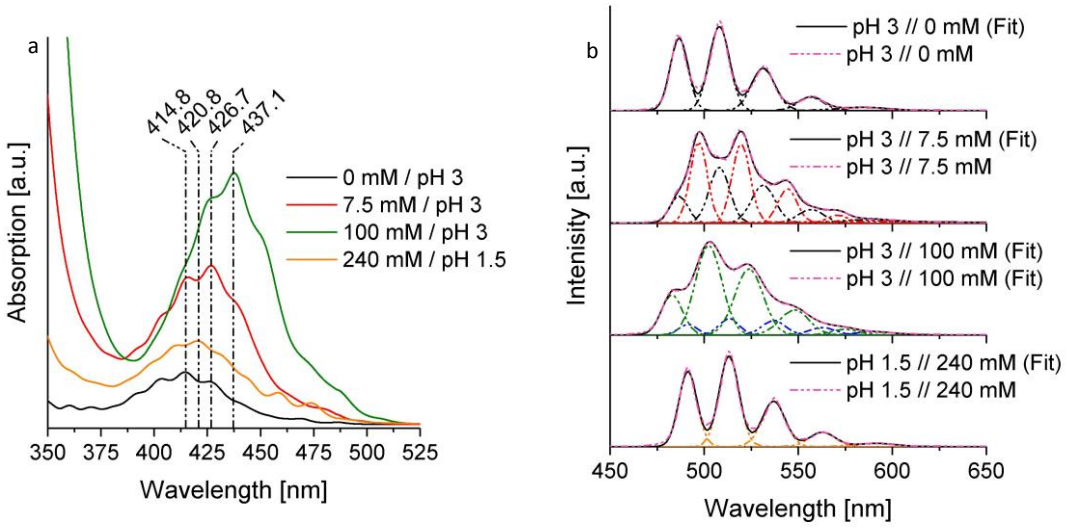

Figure 13: Absorption (a) and related luminescence-spectra (b) of UO_2^{2+}-ISA complexes.

The fact that Species 2 was always dominant at lower pH values, might indicate an unexpected interaction between UO_2^{2+} and HISA. This assumption was further strengthened by the fact that in

The MIND-project has received funding from the European Union's EUROATOM research and training program (Horizon2020) under grant agreement 661880.

the presence of UO_2^{2+}, more of ISL was present in solution up to pH 3. This was observed, when the ATR-FTIR-spectra of the UO_2^{2+}-containing solutions were evaluated with ITFA. The component-distribution either with or without UO_2^{2+} is depicted in Figure A 9. A suitable explanation is based on the lactone-formation mechanism, which is shown in Figure A 10. The first and rate-limiting step is the protonation of the protonated carboxylic group, leading to a carbenium-ion. Since UO_2^{2+} is also a strong electrophile, it could replace the protons in the mechanism, when the concentration of that catalyst decreases with increasing pH. This is possible until the deprotonated carboxylic group becomes more favoured, due to the mesomeric stabilization of the negative charge.

5.2 Determination of the complex-stoichiometry

In order to estimate the limiting metal to ligand ratio in the formed complexes, the method of continuous variation was applied (*47*), which is commonly known as Job Plot. Therefore, absorption spectra were recorded at pH 4 and different metal to ligand ratios, ranging from 1:0 to 1:3.7 (Figure 14). The absorption at 438 nm, the maximum of Species 4, was then plotted against the mole fraction of U(VI). As depicted in Figure 14b, the reflection is at 0.33, which is indicative for a metal to ligand ratio of 1:2. But it has to be mentioned that a complex with a ratio of 2:4 or higher is also possible, since this cannot be distinguished with this method.

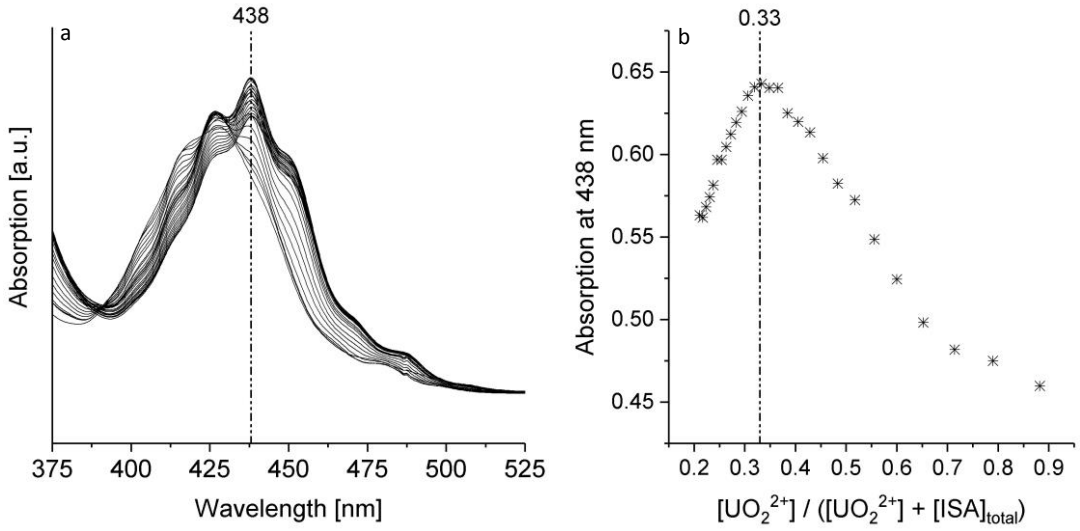

Figure 14: Absorption spectra of UO_2^{2+}-ISA-samples with metal to ligand ratios varying from 1:0 to 1:3.7 at pH 4 (a); Job Plot for absorption at 438 nm (b).

5.3 Determination of the binding motifs

5.3.1 NMR-spectroscopy

Figure 15 shows the superimposed ^{13}C-NMR spectra of free ISA and a sample containing UO_2^{2+} and ISA in a ratio of 1 to 2 at pH 4.2. Clear changes occur in the chemical shifts of certain carbons. The HSQC-NMR spectrum (Figure A 11) allows proper assignments of the carbons in the ^{13}C-NMR spectrum, which were summarized in Table 7.

The MIND-project has received funding from the European Union's EUROATOM research and training program (Horizon2020) under grant agreement 661880.

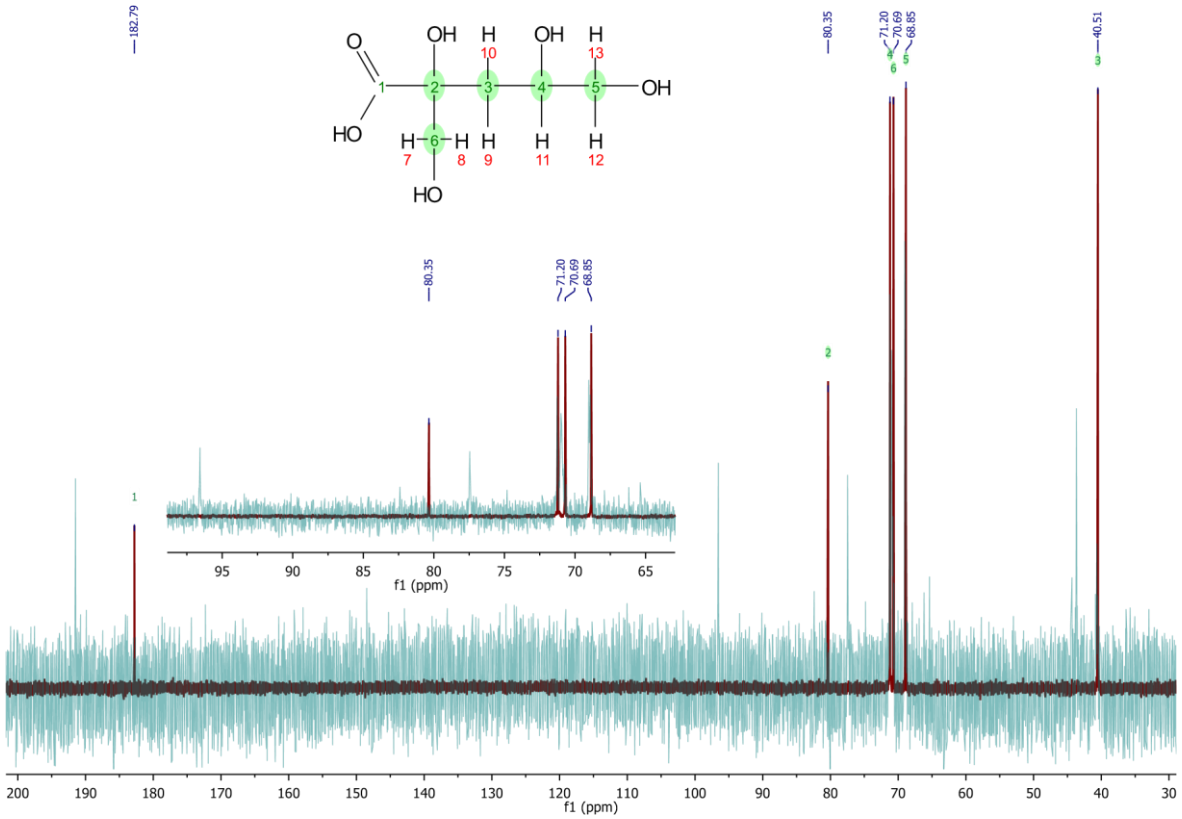

Figure 15: ^{13}C-NMR spectra of free ISA (red) and a UO_2^{2+}-ISA sample (blue) (M:L ratio is 1:2 at pH 4.2).

Table 7: Comparison between experimental ^{13}C-NMR chemical shifts of ISA with and without UO_2^{2+}.

Carbon	Experimental chemical shift in ppm without UO_2^{2+}	Experimental chemical shift in ppm with UO_2^{2+}
3	40.5	43.7 + 40.7
5	68.9	69.0
6	70.7	77.5
4	71.2	71.3
2	80.4	96.6
1	182.8	191.5

C_1, C_2 and C_6 show significantly increased chemical shifts in the presence of UO_2^{2+}.This can be explained with the decreased electron density around these related functional groups, due to the complexation of UO_2^{2+}. This decreased electron density leads to a decreased shielding of the magnetic field and therefore to a higher chemical shift, mentioned earlier. Based on these findings, a chelate binding of UO_2^{2+} via the carboxylic group (C_1) and either the C_2-(3°)- or the C_6-(1°)-alcohol, resulting in a 5- or 6-membered ring, can be expected.

The MIND-project has received funding from the European Union's EUROATOM research and training program (Horizon2020) under grant agreement 661880.

5.3.2 ATR-FTIR-spectroscopy

To identify the binding motifs, samples with different metal to ligand ratios were measured at pH 3 and 4 (Figure 16). The dashed lines in Figure 16c and d indicate the positions of the symmetric and asymmetric stretching of the carboxylic group, the C–O stretching of one 1°, the 2° and the 3° alcohols of the free ISA. At both pH values and all metal to ligand ratios a shift of the asymmetric stretching mode of the carboxylic group to higher (from 1583 cm^{-1} to 1614 cm^{-1}) as well as a shift of the symmetric stretching mode to lower wavenumbers (from 1413 cm^{-1} to 1386 cm^{-1}) was observed. The difference increased from 170 cm^{-1} in the free ISA to 228 cm^{-1} in UO_2^{2+}-ISA complexes. This behavior of these stretching modes is indicative for a monodentate coordination of the carboxylic group to the UO_2^{2+}-entity. Kakihana *et al.* investigated the changes of the respective bands in carboxylic and hydroxy-carboxylic acids (*48*). They observed the above-mentioned pattern for the latter ones, whereas a reversed shift was observed in the case of a bidentate coordinated carboxylic group, namely a decreased distance between the asymmetric and symmetric stretching.

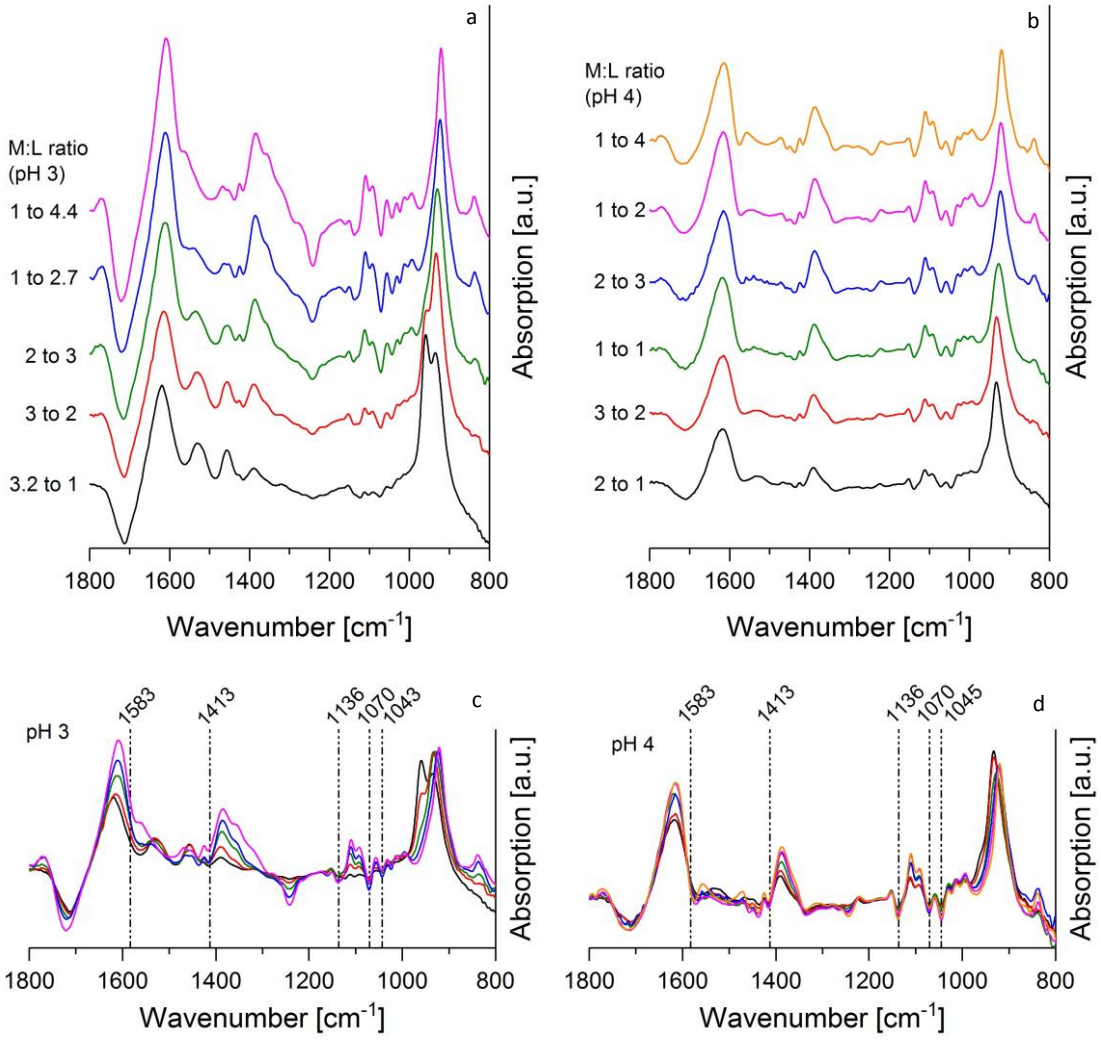

Figure 16: ATR-FTIR-difference spectra of UO_2^{2+}-ISA samples at different metal to ligand ratios: stacked spectra at pH 3 (a) and 4 (b), superimposed spectra at pH 3 (c) and 4 (d).

Several positive and negative bands occur in Figure 16 in the range between 1150 cm^{-1} and 1000 cm^{-1}, where the C–O-stretching modes of the alcohols are located. Clear negative bands can be observed at 1136 cm^{-1}, 1070 cm^{-1} and 1043 cm^{-1}, representing the 3°, the 2° and probably the 1°

The MIND-project has received funding from the European Union's EUROATOM research and training program (Horizon2020) under grant agreement 661880.

alcohol in β-position to the carboxylic group (at C_6). Since the spectra of NaISA-solutions under certain conditions were subtracted from the spectra containing UO_2^{2+}, the mentioned negative bands represent the functional groups which are involved in complex-formation. Due to the changed electron-density, resulting from the interaction with UO_2^{2+}, properties of the related chemical bonds, like bond length and strength were changed. This in turn ends up in a different position of the vibrational mode and therefore in positive bands in the difference spectra. All these information indicate the existence of two dominant binding sites, between the carboxylic group and either the 3° (C_1) or the 1° alcohol (C_6), resulting in a 5- or 6-membered ring. The structural schemes as well as the optimized structures of the corresponding 1:1 complexes for each binding motif are depicted in Figure 17.

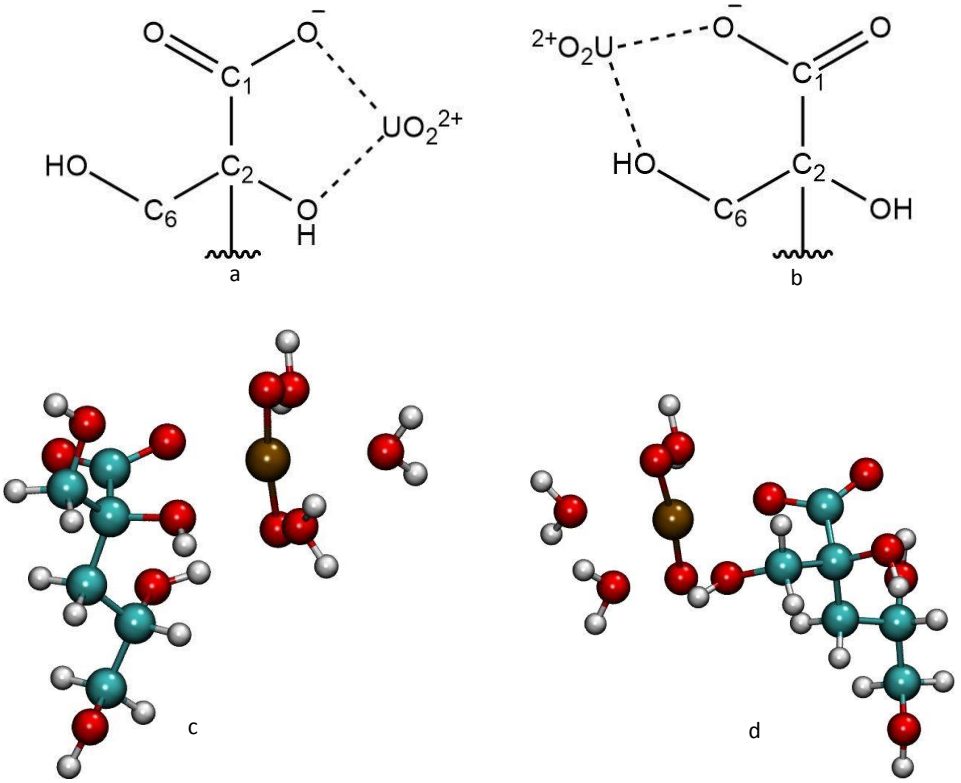

Figure 17: Dominant binding sites in UO_2^{2+}-ISA-complexes: general structure of the 5- (a) and 6-membered ring (b); optimized structures of the $[UO_2ISA]^+$-complex with a 5- (c) and 6-membered ring (d).

5.4 Summary and outlook

Fundamental information about the interaction of UO_2^{2+} with ISA were gathered by a variety of spectroscopic techniques. Undoubtedly are the following information essential to completely describe this system:

- Three dominant UO_2^{2+}-ISA-complexes were discovered
- Two of the three complexes are probably polynuclear
- HISA has to be considered as binding partner up to pH 3
- 5- and 6-membered rings are the dominant binding motifs
- The limiting metal to ligand ratio is 1:2

The MIND-project has received funding from the European Union's EUROATOM research and training program (Horizon2020) under grant agreement 661880.

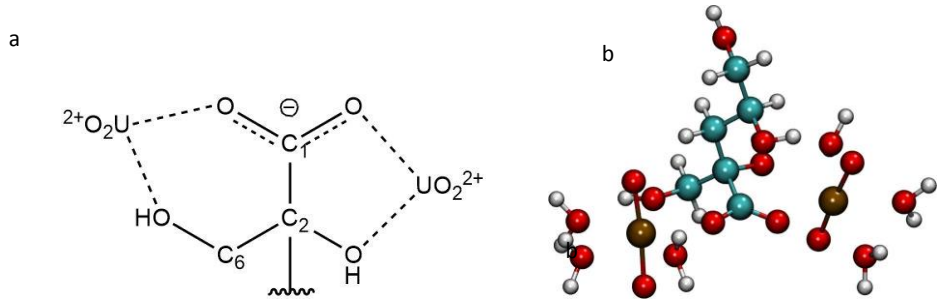

Figure 18: Structure of a 2:1-complex with 5- and 6-membered ring: general (a) and optimized structure (b).

Since the indications for the 5- and 6-membered rings in the ATR-FTIR- and NMR-spectra occur simultaneously it is so far not possible to say if the 1:1 complexes depicted in Figure 17 coexisted together or if complexes were present, having both binding sites. A possible structure is shown in Figure 18. Based on these three building blocks, an almost endless number of conceivable complex-structures are possible. The formation of chain-like structures as well as bridged complexes like in Figure 19 seems to be realistic.

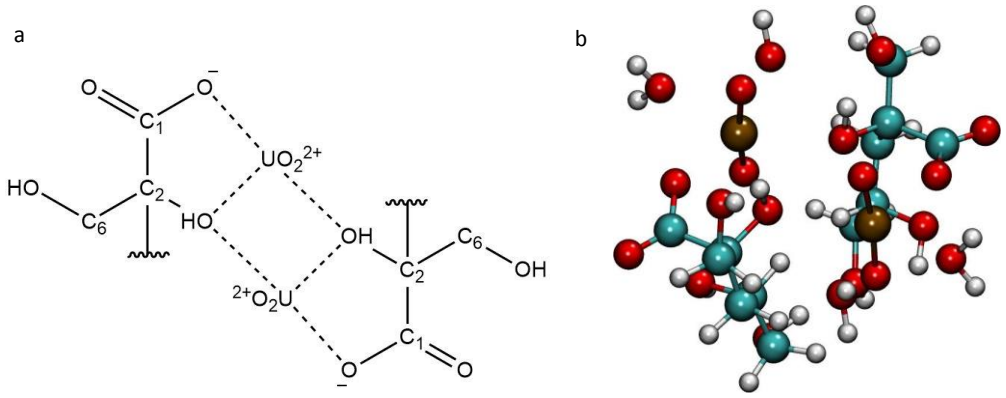

Figure 19: Structure of a 2:2-complex with two 5-membered rings: general (a) and optimized structure (b).

An approach to identify the formed complexes was to compare the experimentally determined relative shift of the asymmetric stretching mode of the UO_2^{2+}-entity with theoretically calculated shift. Figure 20 shows the related region of the ATR-FTIR-spectra of four selected samples. The absorption spectra verified the dominance of either Species 1, 2, 3 or 4 in these samples. Species 2 shows a relative shift of $-12.9\ cm^{-1}$, Species 3 $-23.9\ cm^{-1}$ and Species 4 of $-38.4\ cm^{-1}$. Table 8 summarizes the calculated relative shifts of conceivable optimized complexes.

The MIND-project has received funding from the European Union's EUROATOM research and training program (Horizon2020) under grant agreement 661880.

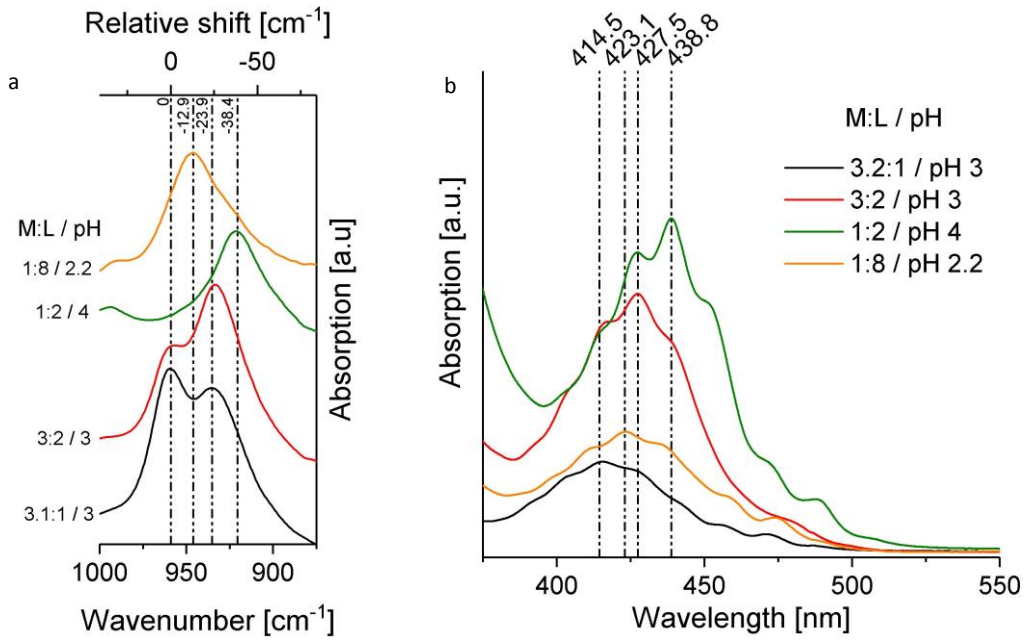

Figure 20: Experimental relative shift of the asymmetric UO_2^{2+}-stretching mode in ISA-complexes: Experimental ATR-FTIR-data (a) and related absorption spectra (b).

Table 8: Calculated relative shifts of the UO_2^{2+}-asymmetric stretching mode in UO_2^{2+}-ISA-complexes

Metal to ligand ratio	Number of H_2O-molecules	Binding sites [a]	Calculated relative shift [b] in cm^{-1}
1:0	5	-	0
2:1	3 / 3	5 / 6	-6.4 / -8.4
	3 / 3	6 / 5d	-16.4 / -63.7
	3 / 3	5 / 6d	-20.7 / -53.4
	3 / 3	6d / 5d	-63.4 / -71.3
1:1	3	4	-18.1
	3	5	-36.2 / -39.5
	3	5d	-81.9 / -93.2
	3	6	-26.4
2:2	2 / 2	5 / 5	-19.8 / -28.0
	2 /2	5 / 5	-9.3 / -13.7
	2 / 2	5 / 6	-37.6 / -47.8

The MIND-project has received funding from the European Union's EUROATOM research and training program (Horizon2020) under grant agreement 661880.

1:2	2	4 / 4	-35.5
	2	4 / 5	-53.4
	1	4 / 5	-50.0
	2	4 / 6	-36.7
	2	5 / 5	-84.6
	2	6 / 6	-46.0
	1	4c / 5	-25.9

[a] 4: 4-membered ring, 5: 5-membered ring, 6: 6-membered ring, d: deprotonated alcohol, c: protonated carboxylic group [b] asymmetric stretching of $[UO_2(H_2O)_5]^{2+}$ subtracted from the respective UO_2^{2+}-ISA complex

Unfortunately does no calculated relative shift fit perfectly to the experimentally observed shifts, while fulfilling the spectroscopically determined properties. Instead of trying to find the ideal complexes based on speculative suggestions, other approaches are necessary to extend the knowledge derived so far from spectroscopy. For this purpose, experiments are running, with the goal to synthesize crystalline UO_2^{2+}-ISA compounds. Then these materials will be characterized by single-crystal-XRD. A second approach is to apply MS to obtain information concerning the mass of the formed complexes, which could dramatically decrease the number of conceivable complex structures. Finally, the ultimate objective is to generate reliable complex formation constants. But to do this properly it is necessary to clarify the speciation in advance.

The MIND-project has received funding from the European Union's EUROATOM research and training program (Horizon2020) under grant agreement 661880.

6 Ongoing studies

- Characterization of U(VI)-ISA interaction under neutral and alkaline conditions
- Investigation of the ternary U-ISA acetate system
- Characterization of the interaction between Eu(III) and ISA
- Investigation of the effect of ISA on the retention of U(VI) by bentonite under neutral and alkaline conditions
- Investigation of the fate of uranium(VI) in the presence of cellulose degradation products under hyperalkaline conditions (cooperation with UNIMAN)

The MIND-project has received funding from the European Union's EUROATOM research and training program (Horizon2020) under grant agreement 661880.

7 References

1. L. Abrahamsen *et al.*, "A review of anthropogenic organic wastes and their degradation behaviour" (2015).

2. R. Guillamont *et al.*, *Update on the Chemical Thermodynamics of Uranium, Neptunium, Plutonium, Americium and Technetium* (2003).

3. C. J. Knill, J. F. Kennedy, Degradation of cellulose under alkaline conditions. *Carbohydr. Polym.* **51**, 281–300 (2003).

4. M. Glaus, L. van Loon, S. Achatz, A. Chodura, K. Fischer, Degradation of cellulosic materials under the alkaline conditions of a cementitious repository for low and intermediate level radioactive waste. Part I: Identification of degradation products. *Anal. Chim. Acta*. **398**, 111–122 (1999).

5. D. Rai, A. Kitamura, Evaluation of equilibrium constants for deprotonation and lactonisation of α-D-isosaccharinic acid. *J. Nucl. Sci. Technol.* **53**, 459–467 (2016).

6. S. Ekberg, C. Ekberg, Y. Albinsson, Characterization of α-Isosaccharinic Acid: Lactone and Carboxylic Conformations. *J. Solution Chem.* **33**, 465–477 (2004).

7. H. Cho, D. Rai, N. J. Hess, Y. Xia, L. Rao, Acidity and Structure of Isosaccharinate in Aqueous Solution: A Nuclear Magnetic Resonance Study. *J. Solution Chem.* **32**, 691–702 (2003).

8. V. Diesen, K. Forsberg, M. Jonsson, Effects of cellulose degradation products on the mobility of Eu(III) in repositories for low and intermediate level radioactive waste. *J. Hazard. Mater.* **340**, 384–389 (2017).

9. M. Felipe-Sotelo *et al.*, Effect of anthropogenic organic complexants on the solubility of Ni, Th, U(IV) and U(VI). *J. Hazard. Mater.* **300**, 553–560 (2015).

10. M. R. González-Siso, X. Gaona, L. Duro, M. Altmaier, J. Bruno, Thermodynamic model of Ni(II) solubility, hydrolysis and complex formation with ISA. *Radiochim. Acta*. **106**, 31–45 (2018).

11. D. Rai, A. Kitamura, Thermodynamic equilibrium constants for important isosaccharinate reactions: A review. *J. Chem. Thermodyn.* **114**, 135–143 (2017).

12. D. Rai, L. Rao, D. A. Moore, The Influence of Isosaccharinic Acid on the Solubility of Np(IV) Hydrous Oxide. *Radiochim. Acta*. **83**, 9–13 (1998).

13. L. Rao, A. Y. Garnov, D. Rai, Y. Xia, R. C. Moore, Protonation and complexation of isosaccharinic acid with U(VI) and Fe(III) in acidic solutions: potentiometric and calorimetric studies. *Radiochim. Acta*. **92**, 575–581 (2004).

14. J. Tits, E. Wieland, M. H. Bradbury, The effect of isosaccharinic acid and gluconic acid on the retention of Eu(III), Am(III) and Th(IV) by calcite. *Appl. Geochemistry*. **20**, 2082–2096 (2005).

15. K. Vercammen, M. A. Glaus, L. R. Van Loon, Complexation of Th(IV) and Eu(III) by α-isosaccharinic acid under alkaline conditions. *Radiochim. Acta*. **89**, 393–401 (2001).

16. K. Vercammen, M. A. Glaus, L. R. Van Loon, Rapid Communication: Evidence for the Existence of Complexes between Th(IV) and α-Isosaccharinic Acid under Alkaline Conditions. *Radiochim. Acta*. **84**, 221–224 (1999).

17. P. Warwick, N. Evans, T. Hall, S. Vines, Stability constants of uranium(IV)-α-isosaccharinic acid

The MIND-project has received funding from the European Union's EUROATOM research and training program (Horizon2020) under grant agreement 661880.

and gluconic acid complexes. *Radiochim. Acta*. **92**, 897–902 (2004).

18. E. Wieland, J. Tits, J. P. Dobler, P. Spieler, The effect of α-isosaccharinic acid on the stability of and Th(IV) uptake by hardened cement paste. *Radiochim. Acta*. **90**, 683–688 (2002).

19. L. R. Whistler, J. N. BeMiller, in *Methods in carbohydrate chemistry* (1963), vol. 2, pp. 477–479.

20. K. Vercammen *et al.*, Complexation of Calcium by alpha-Isosaccharinic Acid under Alkaline Conditions. *Acta Chem. Scand.* **53**, 241–246 (1999).

21. N. M. Bassil, N. Bryan, J. R. Lloyd, Microbial degradation of isosaccharinic acid at high pH. *ISME J.* **9**, 310–320 (2015).

22. L. R. Van Loon, M. A. Glaus, S. Stallone, A. Laube, Sorption of Isosaccharinic Acid, a Cellulose Degradation Product, on Cement. *Environ. Sci. Technol.* **31**, 1243–1245 (1997).

23. P. GANS, A. SABATINI, A. VACCA, Investigation of equilibria in solution. Determination of equilibrium constants with the HYPERQUAD suite of programs. *Talanta*. **43**, 1739–1753 (1996).

24. A. Günther, R. Steudtner, K. Schmeide, G. Bernhard, Luminescence properties of uranium(VI) citrate and uranium(VI) oxalate species and their application in the determination of complex formation constants. *Radiochim. Acta*. **99**, 535–542 (2011).

25. K. Müller, V. Brendler, H. Foerstendorf, Aqueous Uranium(VI) Hydrolysis Species Characterized by Attenuated Total Reflection Fourier-Transform Infrared Spectroscopy. *Inorg. Chem.* **47**, 10127–10134 (2008).

26. S. Ahrland, On the Complex Chemistry of the Uranyl Ion. IV. The Complexity of Uranyl Acetate. *Acta Chem. Scand.* **5**, 199–219 (1951).

27. V. Sladkov, Photochemical characterization of uranyl interaction with acetic acid. *J. Photochem. Photobiol. A Chem.* **295**, 40–45 (2014).

28. V. Sladkov, J. Roques, Deactivation of lowest excited state of uranyl in the presence of acetate: A DFT exploration. *J. Photochem. Photobiol. A Chem.* **322–323**, 10–15 (2016).

29. G. Meinrath, D. Kwiatek, Z. Hnatejko, S. Lis, Direct spectroscopic speciation of the complexation of U(VI) in acetate solution. *Monatshefte für Chemie - Chem. Mon.* **145**, 1689–1696 (2014).

30. Z. Libuś, Absorption spectra of uranium (VI) complexes in solutions. *J. Inorg. Nucl. Chem.* **24**, 619–631 (1962).

31. C. Lucks *et al.*, Aqueous Uranium(VI) Complexes with Acetic and Succinic Acid: Speciation and Structure Revisited. *Inorg. Chem.* **51**, 12288–12300 (2012).

32. D. L. Parkhurst, C. A. J. Appelo, in *U.S. Geological Survey Techniques and Methods, book 6, chapter A43* (2013; https://pubs.usgs.gov/tm/06/a43/).

33. I. Grenthe *et al.*, *Chemical Thermodynamics of Uranium* (1992).

34. P. L. Brown, H. Wanner, “Predicted formation constants using the unified theory of metal ion complexation” (1987).

The MIND-project has received funding from the European Union’s EUROATOM research and training program (Horizon2020) under grant agreement 661880.

35. B. Drobot *et al.*, Combining luminescence spectroscopy, parallel factor analysis and quantum chemistry to reveal metal speciation – a case study of uranyl(<scp>vi</scp>) hydrolysis. *Chem. Sci.* **6**, 964–972 (2015).

36. J. Bell, R. Biggers, The absorption spectrum of the uranyl ion in perchlorate media. *J. Mol. Spectrosc.* **18**, 247–275 (1965).

37. G. Meinrath, D. Kwiatek, Z. Hnatejko, S. Lis, Direct spectroscopic speciation of the complexation of U(VI) in acetate solution. *Monatsh Chem*. **145**, 1689–1696 (2014).

38. P. B. Shaw, Studies of the Alkaline Degradation of Cellulose and the Isolation of Isosaccharinic Acids, 271 (2013).

39. A. Roßberg, T. Reich, G. Bernhard, Complexation of uranium(VI) with protocatechuic acid. Application of iterative transformation factor analysis to EXAFS spectroscopy. *Anal. Bioanal. Chem.* **376**, 631–638 (2003).

40. J. D. S. Goulden, Infra-red spectra of lactates in aqueous solution. *Spectrochim. Acta*. **16**, 715–720 (1960).

41. G. Cassanas, M. Morssli, E. Fabrègue, L. Bardet, Vibrational spectra of lactic acid and lactates. *J. Raman Spectrosc.* **22**, 409–413 (1991).

42. M. Morssli, G. Cassanas, L. Bardet, B. Pauvert, A. Terol, Vibrational analysis of sodium α-, β- and γ-hydroxybutyrates. Inter- and intramolecular hydrogen bonds. *Spectrochim. Acta Part A Mol. Spectrosc.* **47**, 529–541 (1991).

43. J. M. Chalmers, p. R. Griffiths, *Handbook of Vibrational Spectroscopy* (2002).

44. J.-J. Max, C. Chapados, Infrared Spectroscopy of Aqueous Carboxylic Acids: Comparison between Different Acids and Their Salts. *J. Phys. Chem. A*. **108**, 3324–3337 (2004).

45. G. Meinrath, M. Schweinberger, Hydrolysis of the Uranyl(VI) Ion - A Chemometric Approach. *Radiochim. Acta*. **75**, 205–210 (1996).

46. P. Lubal, J. Havel, Spectrophotometric and Potentiometrie Study of Uranyl Hydrolysis in Perchlorate Medium. Is Derivative Spectrophotometry Suitable for Search of the Chemical Model. *Chem. Pap.* **51**, 213–220 (1997).

47. J. S. Renny, L. L. Tomasevich, E. H. Tallmadge, D. B. Collum, Method of Continuous Variations: Applications of Job Plots to the Study of Molecular Associations in Organometallic Chemistry. *Angew. Chemie Int. Ed.* **52**, 11998–12013 (2013).

48. M. Kakihana, T. Nagumo, M. Okamoto, H. Kakihana, Coordination structures for uranyl carboxylate complexes in aqueous solution studied by IR and carbon-13 NMR spectra. *J. Phys. Chem.* **91**, 6128–6136 (1987).

49. R. Brückner, *Reaktionsmechanismen* (Springer Berlin Heidelberg, Berlin, Heidelberg, 2004; http://link.springer.com/10.1007/978-3-662-45684-2).

The MIND-project has received funding from the European Union's EUROATOM research and training program (Horizon2020) under grant agreement 661880.

8 Appendices

Figure A 1: Preparation of ISA I: (a) flushing with argon; (b) after addition of α-lactose monohydrate and $Ca(OH)_2$; (c): after 1 h stirring under argon flush; (d) after 3 d stirring at RT.

Figure A 2: Preparation of ISA II: (a) boiling under reflux; (b) filtering while hot; (c): bright precipitate; (d): precipitate after washing with water and ethanol (before drying).

The MIND-project has received funding from the European Union's EUROATOM research and training program (Horizon2020) under grant agreement 661880.

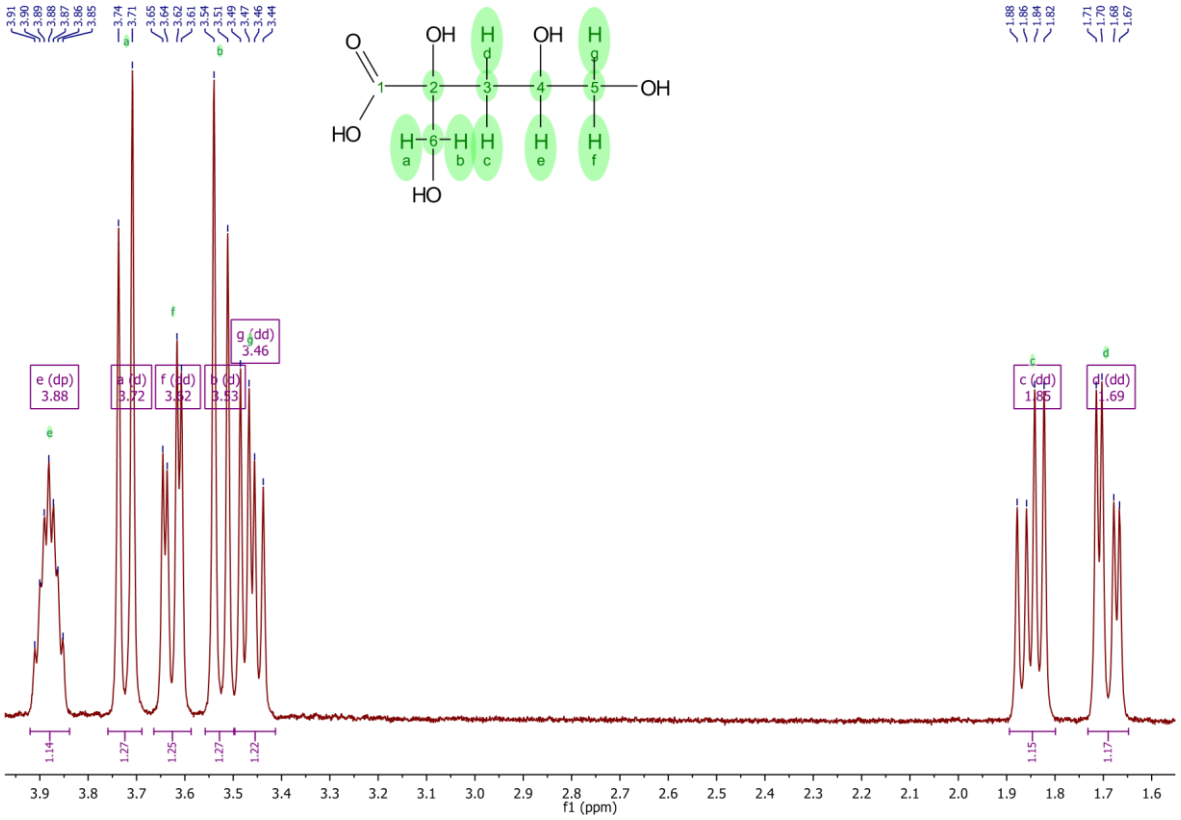

Figure A 3: ^{1}H-NMR spectrum of NaISA stock solution.

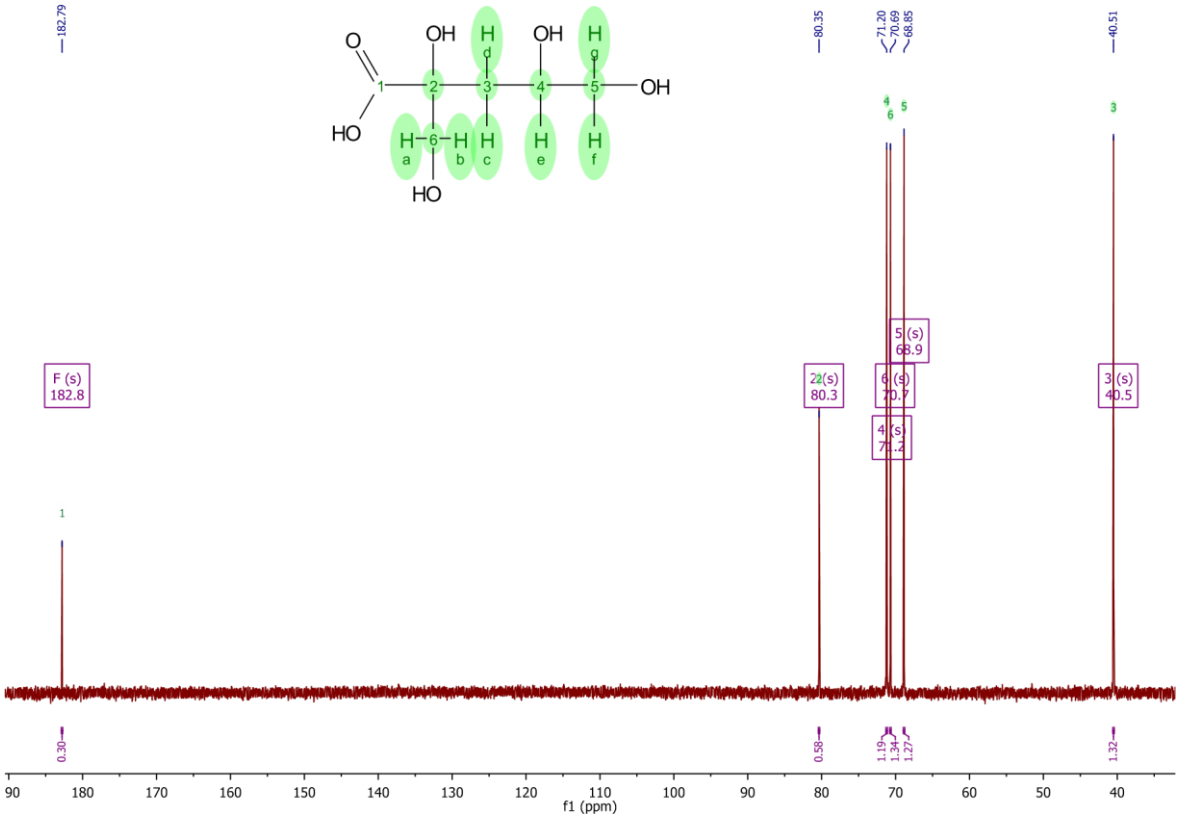

Figure A 4: ^{13}C-NMR spectrum of NaISA stock solution.

The MIND-project has received funding from the European Union's EUROATOM research and training program (Horizon2020) under grant agreement 661880.

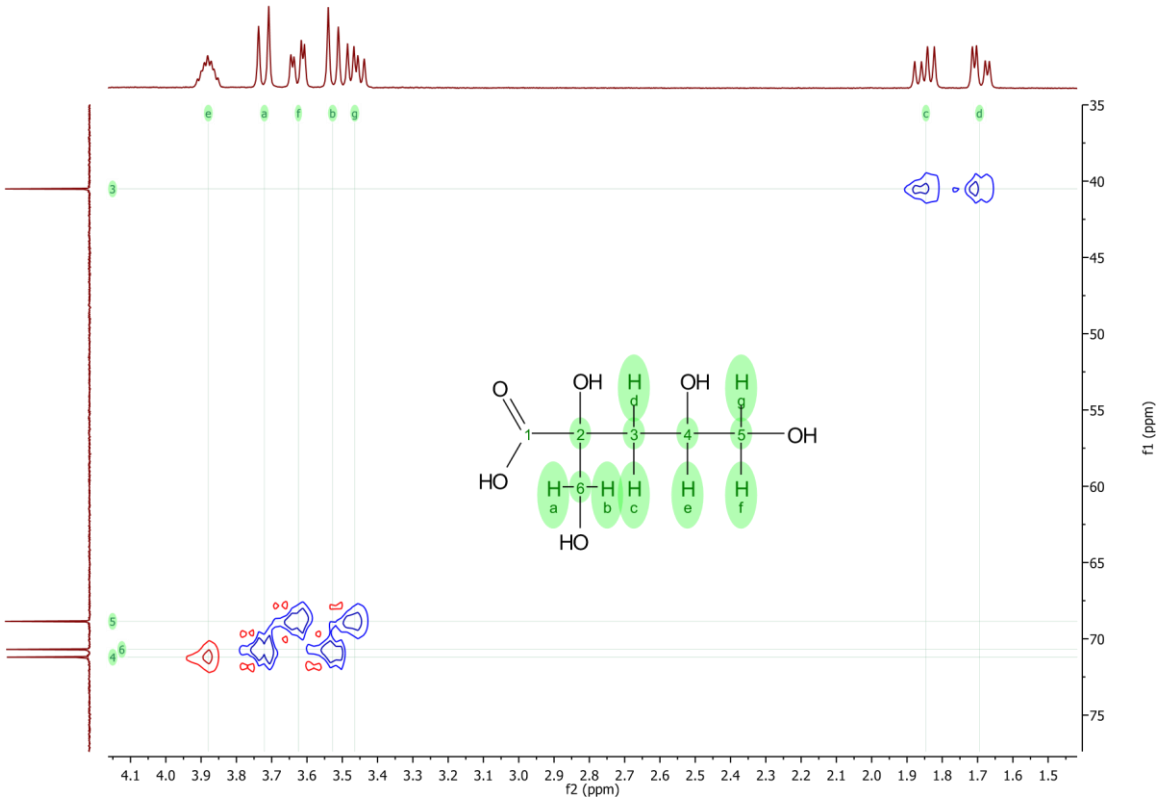

Figure A 5: HSQC-NMR spectrum of NaISA stock solution.

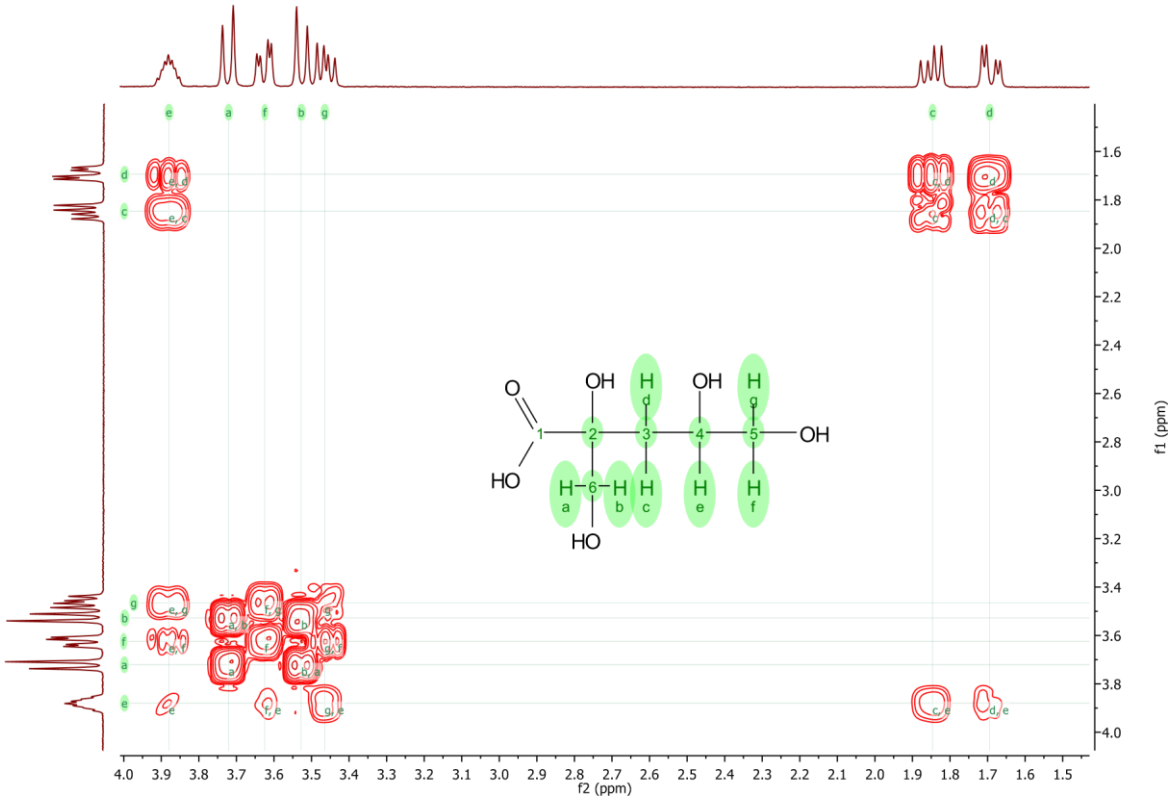

Figure A 6: COSY-NMR spectrum of NaISA stock solution.

The MIND-project has received funding from the European Union's EUROATOM research and training program (Horizon2020) under grant agreement 661880.

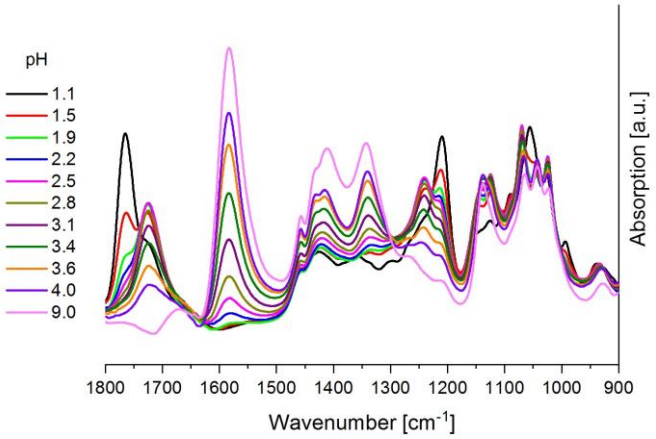

Figure A 7: ATR-FTIR spectra of 90 mM NaISA-solutions at different pH values (I = 1 M NaCl).

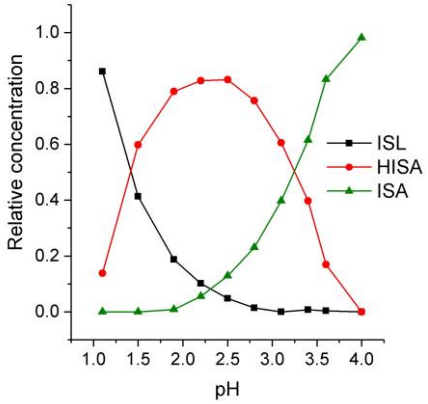

Figure A 8: ITFA derived relative concentrations of ATR-FTIR spectra.

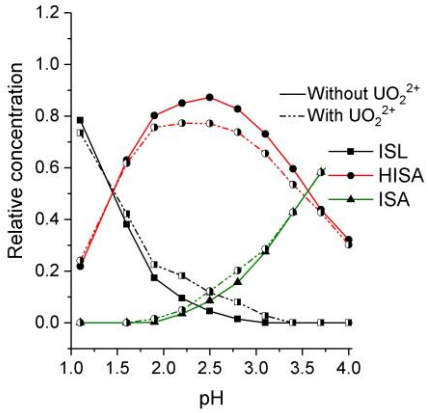

Figure A 9: ITFA derived relative concentrations of ATR-FTIR spectra in the presence of UO_2^{2+}.

The MIND-project has received funding from the European Union's EUROATOM research and training program (Horizon2020) under grant agreement 661880.

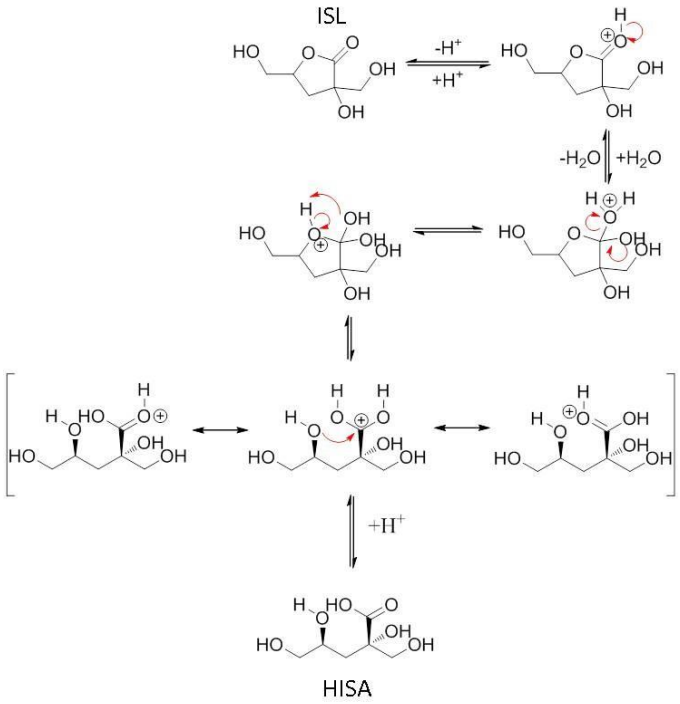

Figure A 10: Lactone formation mechanism according to (49).

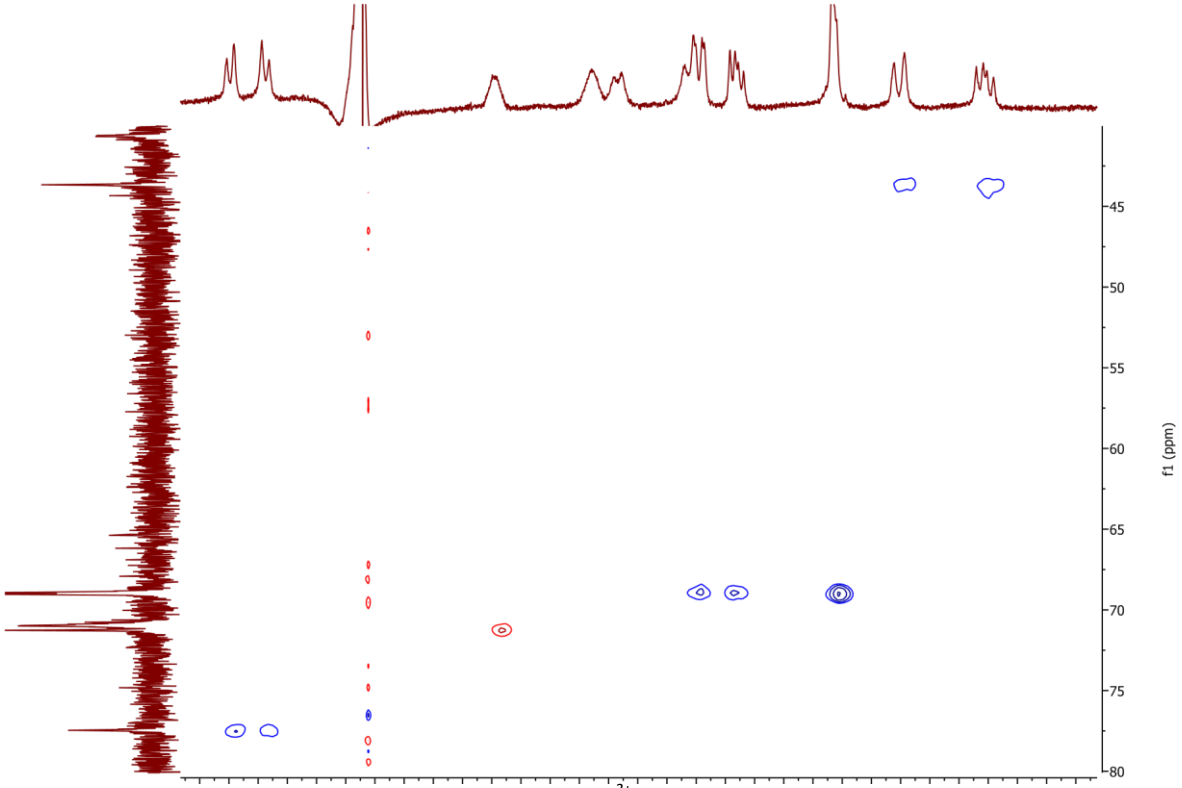

Figure A 11: HSQC-spectrum of an UO_2^{2+}-ISA sample (M:L is 1:2, pH 4.2).

The MIND-project has received funding from the European Union's EUROATOM research and training program (Horizon2020) under grant agreement 661880.